ISSN 2706-655X Vol.3, Issue 8: 25-38, DOI: 10.25236/IJFET.2021.030805

Autonomous Positioning and Control System of Rotor UAV Based on Machine Vision

Chunrun Guo[1,a], Xiaojun Liu[1,2,b*]

[1]School of Electromechanical and Automobile Engineering, Huanggang Normal University, Huanggang 438000, Hubei, China
[2]Hubei Zhongke Research Institute of Industrial Technology, Huanggang 438000, Hubei, China
[a]2019280340130@smail.hgnu.edu.cn, [b]18623582@qq.com
**Corresponding author*

Abstract: *In recent years, with the rapid development of electronic technology and image recognition technology, target recognition technology based on rotary wing UAV has become a hot research topic. This paper mainly studies the autonomous positioning and control system of rotary-wing UAV based on machine vision. This paper uses the weighted average method to convert the color images collected by the camera into grayscale images. The color image collected by the airborne camera is grayed out, and the binary image is obtained after threshold segmentation. The median filter technology is used to eliminate the noise, the edge information of the mark is detected, and the Harris corner points are finally extracted. After the clustering operation is completed, the traditional least squares method is used to fit a straight line, each connected component is matched, and each point is weighted according to its gradient. In this paper, the RANSAC algorithm is used to remove the mismatch points and obtain the SIFT characteristic information. At the same time, the PID control algorithm is used to obtain the deviation required for PID control. According to the rotational speed of the four motors of the deviation control system, the attitude control of the aircraft is realized. Finally, the positioning accuracy of the system is evaluated. Experimental results show that the detection time of SIFT feature points is about 100ms. The results show that machine vision improves the positioning accuracy of rotary-wing UAV and improves the accuracy of target recognition.*

Keywords: *Machine Vision, Rotary Wing Drone, Autonomous Positioning, Control System, Target Recognition*

1. Introduction

In recent years, quadrotor UAVs have attracted more and more attention. Quadrotor UAV is a kind of rotorcraft. The four-rotor UAV has a compact structure and uses four symmetrically distributed rotors to provide power through a brushless motor; the two propellers on the same diagonal have the same rotation direction, and the propellers on different angles rotate in the opposite direction. In particular, if rotor drones can be used instead of manual to implement autonomous and intelligent inspections of high-voltage transmission lines, it will not only save human resources, but also improve the inspection efficiency of transmission lines and avoid manual inspections caused by inspection personnel. Objective factors such as fatigue, experience and technology affect the inspection results.

After the UAV identifies and discovers the target through various airborne sensors, it conducts stable tracking reconnaissance under the premise of maintaining a certain safe distance and not being found. Compared with the traditional tracking mode of sending reconnaissance vehicles and personnel, UAV tracking has the advantages of vision and terrain, and is more secure. At the same time, the UAV can automatically track the target through the algorithm embedded in the airborne processor. At the same time, it can greatly improve the success rate and accuracy of tracking. The main task of visual navigation for UAV terminal collision recovery is to calculate the relative position and attitude of UAV and landing site in real time from sequence images, and then transmit the information to guidance and control system, so as to realize UAV flying to target point and realize accurate recovery and recovery.

Machine vision can greatly improve the accuracy of autonomous positioning of drones. Sun TH believes that machine vision is an excellent tool for inspecting various items such as textiles, fruits, printed circuit boards, electrical components, labels, integrated circuits, and machine tools. He proposed an intelligent system that combines machine vision with artificial intelligence networks. He

ISSN 2706-655X Vol.3, Issue 8: 25-38, DOI: 10.25236/IJFET.2021.030805

proposed an effective inspection process to detect four common defects, including black spots, small ends, flash and peeling during the production of thermal fuse. There are some flaws in his research content [1]. Jiang H developed a gesture interface based on machine vision to provide an alternative method for people with upper limb injuries to perform laboratory tasks that require physical manipulation components. He constructed a 3-D particle filter framework based on color and depth, with a unique description function for facial and hand representation. The framework has been integrated into an interactive model that uses spatial and motion information to effectively deal with occlusion and its negative effects. The method he proposed solves the problem of false merging and false labeling when tracking through occlusion. He then used the same feature coding technology to detect, track and recognize the user's hand. The algorithm he uses is not accurate [2]. Favret C believes that for a long time, computers have been seeking to automatically identify insect species to support activities such as environmental monitoring, forensics, pest diagnosis, border security, and vector epidemiology. He tried to test the scalability of the automatic identification method based on the number of reference samples used to train the classifier and the number of classification units to which the classifier should allocate unknown samples. In order to test the scalability of automatic insect recognition companies, he used sparse processing technology and support vector machines to test the largest data set to date: 72 species of fruit flies and 76 species of mosquitoes. His research lacks necessary experimental data [3]. Aiming at the low error rate and low efficiency caused by traditional manual inspection in clothing size measurement, Li P proposed a clothing size measurement system based on machine vision. He designed the hardware and software systems of the measurement system. The main function of the system hardware is to realize the collection of clothing images through the CCD camera. The core of the whole system is the software part of the system. He uses corner detection algorithms to extract and locate feature points. Aiming at the Forstner algorithm that needs to scan each image pixel, which results in a slower detection speed, he uses the SIFT algorithm to quickly filter the images. He uses coordinate value positioning to analyze key corner positions, and uses proportional calculations to measure the size of clothes. He uses a friendly interface to display the size measurement results. His research is not innovative and not high [4].

In this paper, aiming at the nonlinear, highly coupled and underactuated dynamic model of small four rotor UAV, different control strategies are designed by using different theoretical methods, and the effectiveness of the designed controller in the control system of small four rotor UAV is verified by MATLAB simulation. By analyzing the dynamic process of aircraft and neglecting some secondary factors, the mathematical model of aircraft based on Newton Euler equation is established. According to the characteristics of UAV control system, a multi loop cascade control algorithm based on Improved PID control algorithm is designed, and then the software program is implemented and verified.

2. Machine Vision and Autonomous Positioning of Drones

2.1 Machine Vision

When the object is close to the camera, the angle of view in the image changes greatly and the pixel moves faster; when the object is far away from the camera, the change of the angle of view on the image is small, and the speed of the pixel moving is slow; when the object is infinitely far away from the camera, the angle change in the image is zero, and the speed of the pixel moving is zero. Thus, the distance between the object and the camera can be calculated according to the angle change and the motion speed [5]. The gradient is defined as the image function f (x, y), and the gradient at the point (x, y) is:

Size:

$$g(x,y)=\sqrt{G_x^2+G_y^2}=\sqrt{\left(\frac{\partial f}{\partial x}\right)^2+\left(\frac{\partial f}{\partial y}\right)^2} \tag{1}$$

Direction:

$$\phi(x,y)=\arctan(G_y/G_x) \tag{2}$$

Laplace operator is a kind of second derivative operator. The Laplacian value of a continuous function f (x, y) at position (x, y) is defined as:

ISSN 2706-655X Vol.3, Issue 8: 25-38, DOI: 10.25236/IJFET.2021.030805

$$\nabla^2 f(x,y) = \frac{\partial^2 f(x,y)}{\partial^2 x} + \frac{\partial^2 f(x,y)}{\partial^2 y} \tag{3}$$

Gaussian filtering can be achieved by taking the convolution and Fourier transform of the sliding window. The expression of the filter processing two-dimensional graph is as follows:

$$h'(x,y) = h(x,y) * G(x,y) \tag{4}$$

$$G(x,y) = \frac{1}{2\pi\sigma^2} \exp\left(-\frac{x^2 + y^2}{2\sigma^2} \right) \tag{5}$$

Among them, $h(x,y)$ represents the original image, and $h'(x,y)$ is the filtered image.

Define the modulus and argument of wavelet transform at scale s as:

$$M_s f(x,y) = \sqrt{\left|W_s^1 f(x,y)\right|^2 + \left|W_s^2 f(x,y)\right|^2} \tag{6}$$

$$A_s f(x,y) = arctg\left(\frac{W_s^2 f(x,y)}{W_s^1 f(x,y)} \right) \tag{7}$$

Although the gray image reduces the color space, the gray image does not reduce the quality of the boundary information in the image. Generally speaking, there are three main conversion formulas for converting color images to grayscale images [6].

The first conversion formula is the average method:

$$Gray(i,j) = \left[R(i,j) + G(i,j) + B(i,j) \right] / 3 \tag{8}$$

The second conversion formula is the maximum method:

$$Gray(i,j) = \max\left(R(i,j), G(i,j), B(i,j) \right) \tag{9}$$

The third conversion formula is the weighted average method:

$$Gray(i,j) = 0.299R(i,j) + 0.587G(i,j) + 0.114B(i,j) \tag{10}$$

Where, Gray (i, j) represents the gray value of pixel (i, j) after graying, and R (i, j), G (i, j) and B (i, j) represent the values of red, green and blue components of source image pixels (i, j) respectively [7].

Edge detection uses Canny edge detection algorithm. According to the convolution theorem in correlation, the Fourier transform of the function cross-correlation is equal to the product of the Fourier transform of the function, and the formula for conversion to the frequency domain is as follows:

$$F(g) = F(f \otimes h) = F(f) \cdot F(h)^* \tag{11}$$

DS Bolme uses the least square method to solve, and its formula is as follows:

$$\min H^* = \sum_{i=1}^{m} \left| H^* F_i - G_i \right|^2 \tag{12}$$

Among them, m represents the number of samples. If the sample vectors in the covariance matrix are independent and identically distributed, then the Mahalanobis distance between the sample vectors can be expressed as:

$$D(X_i, X_j) = \sqrt{(X_i - X_j)^T (X_i - X_j)} \tag{13}$$

Assuming that there are vector $A(x_1, y_1)$ and vector $B(x_2, y_2)$ in the two-dimensional space, the cosine value of the angle between them can be expressed as:

ISSN 2706-655X Vol.3, Issue 8: 25-38, DOI: 10.25236/IJFET.2021.030805

$$\cos\theta = \frac{x_1 x_2 + y_1 y_2}{\sqrt{x_1^2 + y_1^2}\sqrt{x_2^2 + y_2^2}} \tag{14}$$

The cosine distance of the similarity between sample points a and b can be specifically expressed as:

$$\cos\theta = \frac{\sum_{k=1}^{n} x_{1k} x_{2k}}{\sqrt{\sum_{k=1}^{n} x_{1k}^2}\sqrt{\sum_{k=1}^{n} x_{2k}^2}} \tag{15}$$

2.2 Rotor UAV

The four-rotor UAV attitude control loop is responsible for the attitude control of the UAV. PID control is also used, and the angle error is input as the controller to realize the tracking of the desired attitude angle. Tilt-rotor aircraft is not a simple superposition of the rotor and fixed-wing aircraft structure, so in addition to considering the aerodynamic model of each component, it is also necessary to consider the mutual interference between them [8].

The control performance of the PID controller mainly depends on the values of three parameters. The function of the proportional term is to make the error always decrease in the direction of its absolute value. The larger the proportional parameter, the faster the response speed and the better the stability accuracy; too large a proportional parameter will lead to large overshoot and steady-state oscillation. The function of the differential term is equivalent to damping, which always hinders the error change. Increasing the parameters of the differential term can reduce the overshoot and eliminate the steady-state oscillation [9-10]. Through the command channel, we can control the takeoff, landing and emergency stop of quadrotor UAV. We can also set the change rate of pitch angle, roll angle and yaw angle of quadrotor. We can also control the PWM signal of four motors to achieve the effect of controlling motor rotation rate. Generally, the communication frequency of this channel is 30Hz.

The navigation channel mainly obtains information including engine speed, speed, status and other information. This channel can also obtain battery power usage information, and obtain the altitude, yaw angle, pitch angle, and roll angle of the quadrotor through sensors. The video information of the front camera and the lower camera of the quadrotor can be obtained through the video channel. For the UAV ground control station, it is an extremely important part of the entire UAV inspection, and it is also the fundamental channel for realizing the connection between the ground and the air UAV [11].

2.3 Target Positioning and Control System

Rotor UAV control system mainly includes:

(1) Video information acquisition: the four rotor aircraft sends the image information to the ground control platform through the airborne visual sensing equipment.

(2) Image information processing: image information is processed, the purpose is to reduce the interference of noise, so that the image information more robustly reflects the information of the moving target. Processing methods include image processing methods such as color space conversion, de-drying, open operation, and close operation [12].

(3) Moving target detection: the detection of target information is a necessary stage of target tracking. Only when the target information is detected from the diverse and changing environmental information can the tracking be more robust. For example, the recognition method of target template matching.

(4) Target tracking: the improved algorithm is used to predict the position information of the target stably and track the moving target accurately when the background is the same or similar [13].

The scheme design of quadrotor UAV for tracking and positioning motion is shown in Figure 1. The process can be described as follows: the current frame image of landing mark is collected by airborne camera and converted into the image under HSV color model, and the color feature information mainly composed of hue H component and saturation S component is detected. Meanwhile, SIFT feature points of current frame image and target image are extracted and matched, and false matching points are removed by RANSAC algorithm to obtain SIFT feature information. In this

ISSN 2706-655X Vol.3, Issue 8: 25-38, DOI: 10.25236/IJFET.2021.030805

process, when the effective number of particles near the target state is too small, resampling technology is needed to ensure the diversity of particles [14].

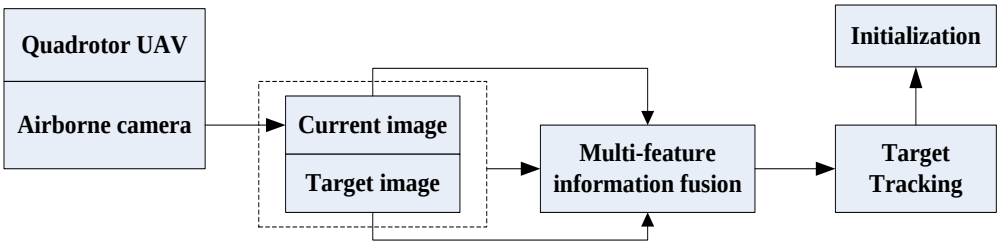

Figure 1: Scheme design of quadrotor UAV for tracking and positioning movement

The image acquisition module is mainly composed of an onboard camera, a two-axis brushless pan/tilt, and a wireless image transmission system. Because the target tracking in this article relies on visual image processing, the definition of image acquisition directly affects the target tracking accuracy of the entire system, so the choice and installation of the camera also directly affect the recognition and positioning of the target. The rate of wireless image transmission and the quality of the return image also affect the performance of the entire system [15].

The controller is the core part of the aircraft, which directly determines the flight performance of UAV. After some initialization, the internal program uses the timer to complete the data acquisition and attitude estimation of each sensor in a fixed time; then uses the control command to complete the drive signal output through the control calculation and motor distribution, and finally sends the required flight data to the ground station by means of wireless data transmission. As the "brain" of quadrotor UAV, the controller also needs to have the performance of quickly processing a large amount of data and storing data, as well as providing more interfaces to facilitate the access of external equipment and the secondary development of flight control [16].

The airborne wireless communication module mainly includes a wireless image sending module and a wireless data transmission module, which respectively send the image information processed by the image processor and the flight status of the quadrotor to the ground station. At the same time, the wireless data transmission module can also receive the control signal sent by the ground station. The ultrasonic ranging module is installed in the center of the quad-rotor UAV and points vertically to the ground to measure the real-time flight height of the quad-rotor UAV and output it to the flight controller module [17-18].

3. Simulation Experiment of Autonomous Positioning and Control System of Rotary Wing Drone

3.1 Experimental Environment

In this paper, the quadrotor UAV is selected as the flight experiment hardware platform, and the zensi Z3 pan tilt camera is used as the image acquisition equipment. GPS is used to obtain its position in real time. And use the manifold magic computing as the core processor to design the software function and realize the code. The core of manifold is NVIDIA's tegrak1 processor, which has a CPU + GPU + ISP architecture, with a maximum frequency of 2.3GHZ. The algorithm is written in C++ and C language, and the test platform is the image processor mentioned above. In the experiment, the parameters of the algorithm remain unchanged for all test videos, and the position of the target center point is saved in .txt text, which is convenient for simulation and analysis in MATLAB [19]. The parameter settings of the algorithm are shown in Table 1.

Table 1: Algorithm parameter settings

Parameter name	Numerical value
Target size	m ×n
One-dimensional filter scale	S ×1
Gaussian kernel standard deviation	0.6
Learning factor	0.012
Regularization parameters	0.0001
Scale factor	1.1
Scale learning factor	0.02

ISSN 2706-655X Vol.3, Issue 8: 25-38, DOI: 10.25236/IJFET.2021.030805

3.2 Image Preprocessing

When the camera collects an image, it is preprocessed to improve the image quality, better highlight the target feature information, remove useless information, and effectively highlight the target from the background. Therefore, this article firstly performs grayscale processing on the image to reduce the data complexity of the image, and then smoothes the image to filter out the interference in the image, enhance the feature information of the target, and improve the effect of subsequent image algorithm processing [20]. This paper uses the weighted average method to convert the color images collected by the camera into grayscale images. The color image collected by the airborne camera is grayed out, and the binary image is obtained after threshold segmentation. The median filter technology is used to eliminate the noise, the edge information of the mark is detected, and the Harris corner point is finally extracted [21].

3.3 Target Recognition

When positioning a target, the input image is generally converted into a grayscale image for calculation. Read the picture and perform image gray-scale processing. In this paper, Gaussian Blur method is used to process grayscale images. Smooth the noise generated when the image is input and the noise generated when the gray image is converted from the original image, so as to reduce the target false detection rate [22]. Then calculate the gradient of each pixel in the image, including the gradient size and gradient direction, and then divide the gradient amplitude of all pixels according to the given threshold M to divide the edge points. Finally, cluster the edge points. After the clustering operation is completed, the traditional least squares method is used to fit a straight line, each connected component is matched, and each point is weighted according to its gradient [23].

3.4 Target Tracking

The current frame image of landing mark is collected by airborne camera and converted into the image under HSV color model. The color feature information of hue H component and saturation S component are detected. The SIFT feature points of current frame image and target image are extracted and matched. The false matching points are removed by RANSAC algorithm, and the SIFT feature information is obtained, and the tracking window is initialized. The texture features of the same image are weighted and fused into the observation information of the tracking target, and the particle filter and CAMSHIFT tracking algorithm are combined to realize the real-time tracking of UAV landing field [24-25].

3.5 Location Parameter Measurement

In order to eliminate the influence of camera distortion on the accuracy of UAV attitude estimation, the camera is first calibrated to obtain the camera's internal parameter matrix. Secondly, using the matched 12 corner point pairs, the corresponding homography matrix can be calculated according to the direct linear transformation, and the homography matrix can be decomposed by non-singular value decomposition, and the rotation matrix R and the translation vector t can be obtained. The matrix solves the attitude angle of the drone. In this paper, the depth of the mark centroid is estimated by the area and perimeter respectively, and the average value is taken as the final mark centroid depth value, and from this, the x and y coordinates of the H-shaped mark centroid relative to the camera's optical center are calculated [26-27].

3.6 Control Algorithm

The four rotor aircraft adopts PID control algorithm. The attitude of the system is detected by the sensor as the feedback value of the system. The deviation required by PID control is obtained by making difference with the attitude value set by the input. According to the rotation speed of the four motors in the deviation control system, the attitude of the aircraft is controlled. The control system uses the timer interrupt form to ensure the fixed frequency of collecting sensor data every 1 millisecond, calculates the attitude data according to the sensor data fusion every 2 milliseconds, and sends out the control information according to the attitude information [28].

ISSN 2706-655X Vol.3, Issue 8: 25-38, DOI: 10.25236/IJFET.2021.030805

3.7 Evaluation Index of System Positioning Accuracy

In this experiment, the quality of the estimated trajectory is evaluated from the given input sequence of the image. This method greatly simplifies the evaluation process. Generally, the relative attitude error at all times is used to calculate the root mean square error of the translation component between the true trajectory and the estimated trajectory at all times. This experiment uses this method to calculate the root mean square error of the shift of the pose translation component in m/s and the mean value of the shift of the pose translation component [29].

4. System Simulation Results

4.1 Effect of Machine Vision on Autonomous Positioning Accuracy of Drones

The effects of adding weight saturation allocator are compared by simulation. The rise time of altitude subsystem when pitch angle and roll angle increase from 0.05rad to 0.8rad are counted respectively. The results are shown in Table 2. It can be seen from the simulation results that the weight allocator eliminates the internal disturbance caused by invalid increment. With the increase of attitude angle, the rise time of height subsystem after adding weight allocator increases slowly, and the system can achieve convergence faster. This combination can not only meet the control requirements of each channel of quav, but also ensure that the control capacity of each channel is not excessive, so as to maximize the utilization rate of control ability, reduce the complexity of the algorithm, and improve the operation efficiency of quav processor. In the simulation, the starting time of each channel input step signal is set as different, so as to observe the mutual influence of each channel.

Table 2: Comparison of system rise time with and without weight distributor

Angle value/rad	Rise time of weightless distributor/s	Rise time of weight distributor/s
0.05	2.0421	2.0424
0.1	2.0431	2.0439
0.2	2.0494	2.0468
0.3	2.0628	2.0534
0.4	2.0788	2.0581
0.5	2.1105	2.0638
0.6	2.1171	2.0734
0.7	2.3061	2.0927
0.8	2.8675	2.2281

The performance test results are shown in Table 3 and Figure 2. It can be seen from the above table that after gray-scale processing, filtering processing, and binarization processing, the sign of the circle is clearly displayed in the black and white image, and the ellipse fitting algorithm can easily identify the circle. Therefore, the system has very strong anti-interference ability, and its performance is superior to the system using corner tracking algorithm and pattern recognition algorithm.

Table 3: Performance test results

Graying processing	0.0545	0.0950	0.0663	0.1005	0.0425	0.0289	0.0958	0.0921	0.0786	0.0366
Filter processing	0.0781	0.0908	0.0408	0.0847	0.0533	0.0841	0.0955	0.0620	0.0355	0.0787
Value processing	0.1142	0.1013	0.0447	0.0494	0.0740	0.0667	0.0366	0.1095	0.0997	0.0650
Ellipse fitting	0.0572	0.0900	0.0736	0.0877	0.0610	0.0708	0.0581	0.0797	0.0830	0.0552

ISSN 2706-655X Vol.3, Issue 8: 25-38, DOI: 10.25236/IJFET.2021.030805

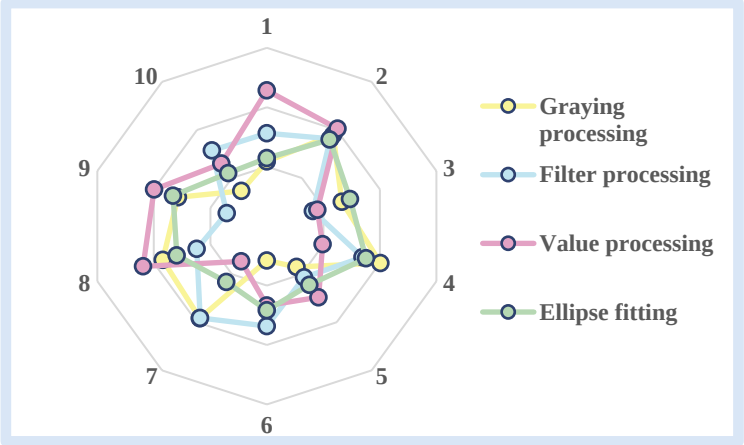

Figure 2: Performance test results

The statistical results of the average calculation time of different numbers of different algorithms in the matlab simulation environment on a PC with general configuration are shown in Figure 3. It can be seen from the above figure that all algorithms except Mirzaei have a calculation speed of less than 5ms when the number of points is relatively small, and they basically meet the real-time requirements. The calculation speed of the RPnL algorithm is the fastest and the calculation time does not change with the number of lines within 15 lines. The time of the RPnL algorithm is 1.788ms with 5 lines, which meets the real-time requirements.

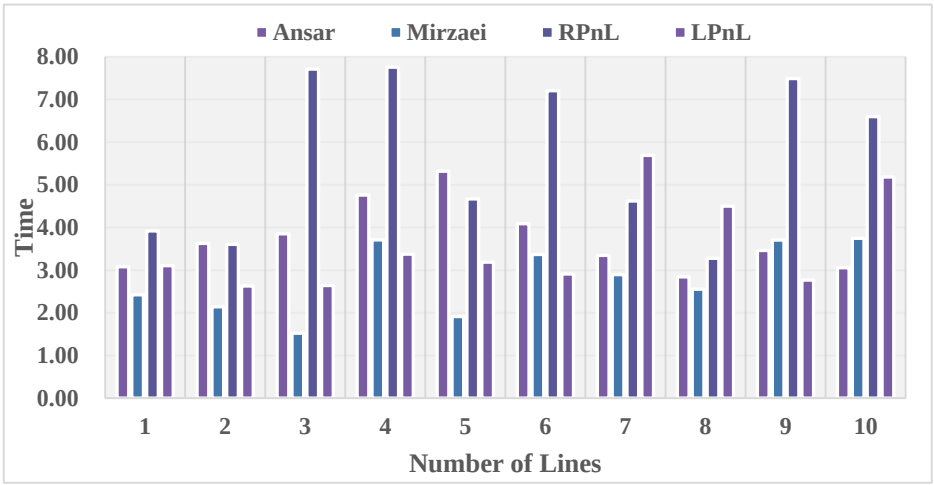

Figure 3: Statistical results of average calculation time for different numbers of bars

The adjustment time and overshoot are shown in Table 4. Because the weight value of neural network nodes is the initial value of PID control parameters, so in the early stage of control, the effect of the two methods on attitude control is similar, but as time goes on, the number of iterations increases, the weight of network structure is worth optimizing, so it shows different control performance from traditional PID. Among them, in the control of roll angle roll, the PIDNN control curve is below the PID control curve in 0 to 0.5s, and the attitude adjustment performance is lower than that of PID, indicating that the network structure is in the process of learning and training during this period. After 48 seconds, the PID controller can quickly adjust the desired value within 1.5 seconds.

Table 4: Adjustment time and overshoot

Comparison of results	Roll		Pitch		Yaw	
	Adjustment time (s)	Overshoot (rad)	Adjustment time (s)	Overshoot (rad)	Adjustment time (s)	Overshoot (rad)
PID	2.82	0	3.06	0	3.16	0.032
PIDNN	1.34	0	2.72	0	2.60	0.008
Optimization ratio	52.5%	0	11.1%	0	17.7%	75%

ISSN 2706-655X Vol.3, Issue 8: 25-38, DOI: 10.25236/IJFET.2021.030805

4.2 Algorithm Performance Analysis

In this paper, three evaluation indexes are used to evaluate the test results of video sequence 2. The test results are shown in Figure 4. It can be seen that when the scale becomes smaller, the camera is farther and farther away from the tracking target, and the algorithm has good adaptability. The scale error can be controlled below 0.12, which means that there is a small error between the area of the tracking frame and the actual area of the target; the pixel error of the center point is about 5 pixels, all below 10 pixels. For a 960 pixel × 544 pixel video sequence, the center pixel error is relatively small; the coverage rate of the tracking frame is more than 0.88, which proves that the engineering tracking frame can cover the whole tracking target more comprehensively. For video sequence 4, the tracking result at 0 frame is not ideal, but with the size of insulator becoming smaller, the pixel error curve of center point is decreasing, and the coverage rate is further improved, which can get better test results. In the end, the tracking frame can cover the tracking target almost completely, but the tracking box is slightly larger than the actual target.

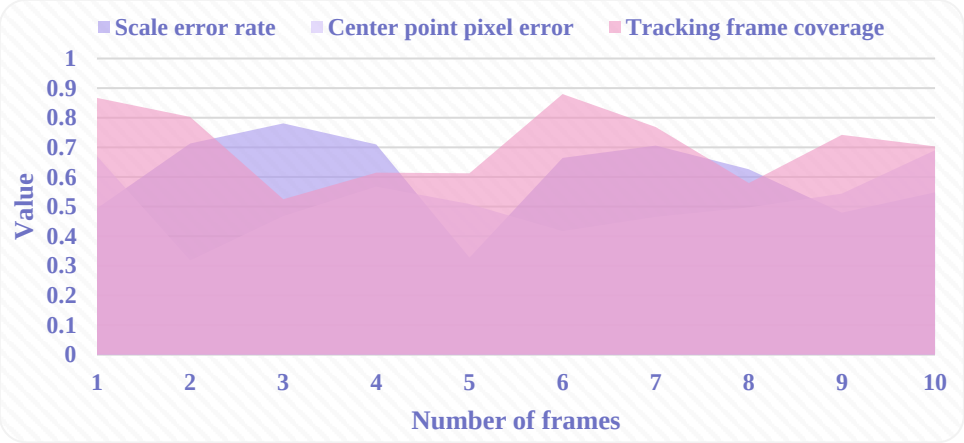

Figure 4: Test results

The frame rate change of the machine vision unit is shown in Figure 5. It can be seen from the figure that the processing rate is about 14 frames, that is, it takes about 70 ms to get a complete position data. Finally, the position data we get is transmitted to the flight control unit, and the control rate of the flight control unit can reach 50Hz under the optimal condition. In addition, considering the transformation from position data to attitude control data and the stability of the system, the tracking loop is set as the triple frequency of the control loop. At the same time, in order to ensure the accuracy of the data, the data verification protection is done in the software. Therefore, the processing performance of machine vision unit can fully meet the system requirements. In addition, the machine vision unit can realize the accurate recognition of the target object at different distances by changing the lens with different focal length.

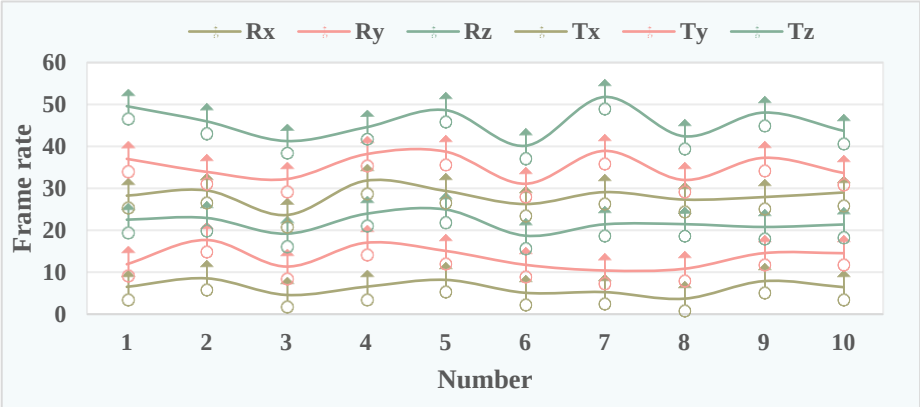

Figure 5: Frame rate change of machine vision unit

The absolute errors of the four distance parameter solutions are shown in Figure 6. From the figure, we can see that the camera lens distortion has a great impact on the accuracy of the solution,

ISSN 2706-655X Vol.3, Issue 8: 25-38, DOI: 10.25236/IJFET.2021.030805

especially the farther the distance, the more serious the lens distortion is, the larger the deviation of the solution results; at the same time, we can see that both the linear algorithm and the nonlinear optimization algorithm can get more accurate results when the UAV is close than when the UAV is far away, and the error is very small. We can see that the result of nonlinear optimization is closer to the curve of real value than the result of linear solution. However, when the linear solution deviates from the real value far, the result of the nonlinear solution will be unstable if the linear solution is substituted into the nonlinear optimization algorithm as the initial value, sometimes it will be optimized to the real value direction, sometimes to the opposite direction. At the same time, we can see that the nonlinear algorithm has a good optimization effect on both distance and angle, but when the effect of distance optimization is strong, the optimization of angle is relatively weak, on the contrary, when the optimization of angle is strong, the optimization of distance is weak.

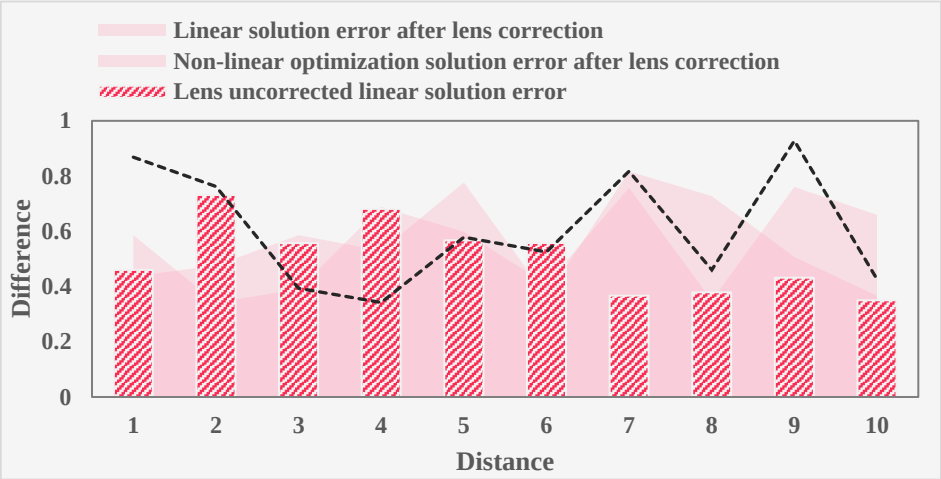

Figure 6: The absolute error of the four distance parameter solutions

4.3 Target Detection Results

The experimental results of different feature point image detection are shown in Table 5 and Figure 7. In SURF detection experiment, the threshold value of Hessian matrix determinant in SURF feature point detection set by OpenCV is 100. Using this default value will detect two to three times more feature points than SIFT detection result. It takes more time and most feature points have poor quality. Therefore, this paper sets it to 1500, which is more commonly used. ORB feature points are also set by default. Since orb feature points are based on fast corner detection, and there are usually tens of thousands of corners detected by fast, it is necessary to limit the number of feature points that can be extracted at most. SIFT usually takes about two thousand seconds to detect features. SURF feature point detection method for different environments, the detection time fluctuation is large, the longest time-consuming is 90.5ms, the shortest is 29.6ms, the number of detected feature points is also large fluctuations, in general, the time consumption and the number of feature points detection are less than SIFT feature point detection. Due to the principle of orb feature point detection algorithm, except for very few cases, the number of feature points detection is relatively fixed, the time consumption is the minimum, and the real-time performance is the highest.

Table 5: Image detection results of different feature points

Serial number	SIFT		SURF		ORB	
	Time-consuming (s)	Quantity	Time-consuming (s)	Quantity	Time-consuming (s)	Quantity
1	0.1338	1912	0.0905	1229	0.0149	500
2	0.1043	1576	0.0399	432	0.0131	500
3	0.1094	1476	0.0475	434	0.0135	500
4	0.103	1458	0.0676	667	0.014	500
5	0.1037	1550	0.0473	347	0.0143	500
6	0.1533	2880	0.0873	1416	0.0158	500
7	0.1187	1792	0.0728	973	0.0144	500
8	0.1135	1843	0.0677	740	0.0147	500

ISSN 2706-655X Vol.3, Issue 8: 25-38, DOI: 10.25236/IJFET.2021.030805

9	0.0678	210	0.0296	110	0.0101	474
10	0.0736	440	0.0338	156	0.0103	500

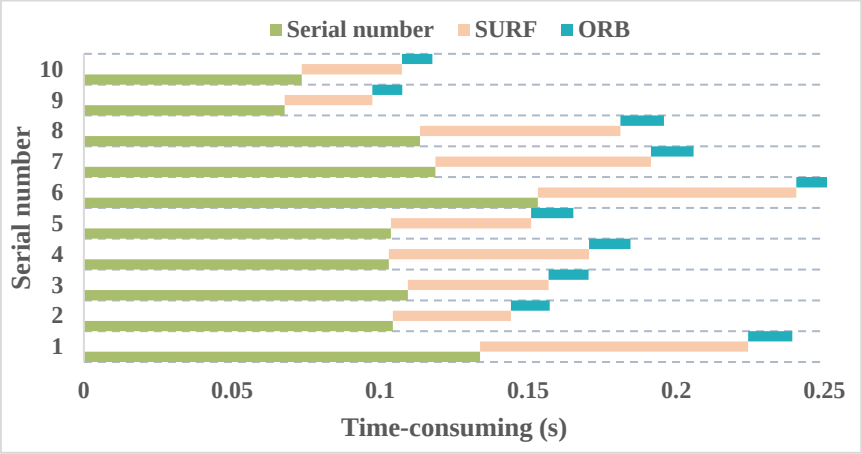

Figure 7: Image detection results of different feature points

The average coverage rate of UAV target recognition is shown in Figure 8. It can be seen from the figure that the algorithm used in this paper has the best tracking effect in the aerial video sequences group2, person1 and UAV2. In the video sequence car2_s, the algorithm used in this paper has a certain drift and loss of targets due to factors such as the fast movement of the target and the interference of the surrounding environment. In the video sequence group2, the center position error of the algorithm used in this article is the smallest, which means that the algorithm used in this article can still track accurately when the target is similar to the surrounding environment and is occluded. The algorithm Staple and the algorithm SiamFC are due to the above interference factors. The tracking task has not been completed greatly. Although the algorithm DSST and the algorithm MDNET occasionally drift, the overall tracking is stable and can continue to track the target.

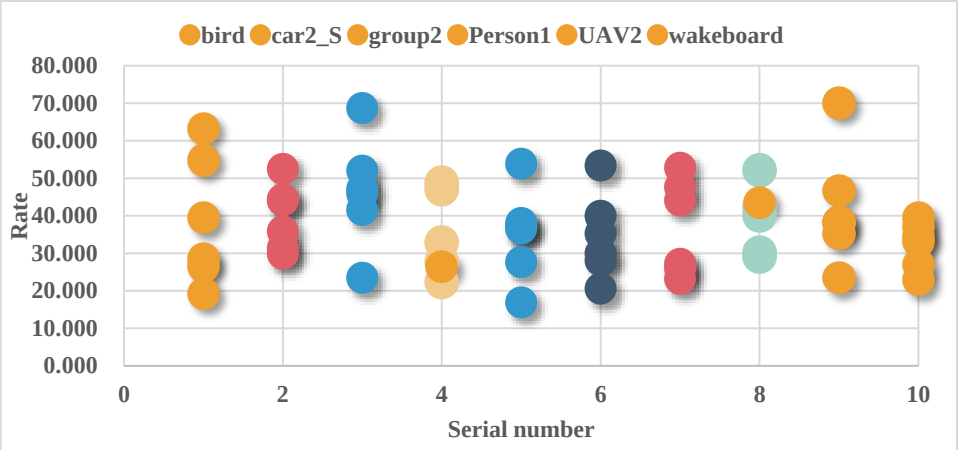

Figure 8: Average coverage

The attitude estimation of the quadrotor UAV is shown in Figure 9. Since the controller uses the estimated value of the attitude as the feedback quantity, there is a certain error in the calculation of the control quantity, and the situation that each attitude angle oscillates at the zero point appears. The drone can track a single square wave signal in the direction of the yaw angle; the acceleration of the drone will change near the step point, and the attitude error will increase at this time. When the drone is restored to balance, the attitude error will also return to the previous status. The above simulation results show that the cascade filter system composed of UKF and multi-sensor complementary filters can effectively realize the attitude estimation of the quad-rotor UAV.

ISSN 2706-655X Vol.3, Issue 8: 25-38, DOI: 10.25236/IJFET.2021.030805

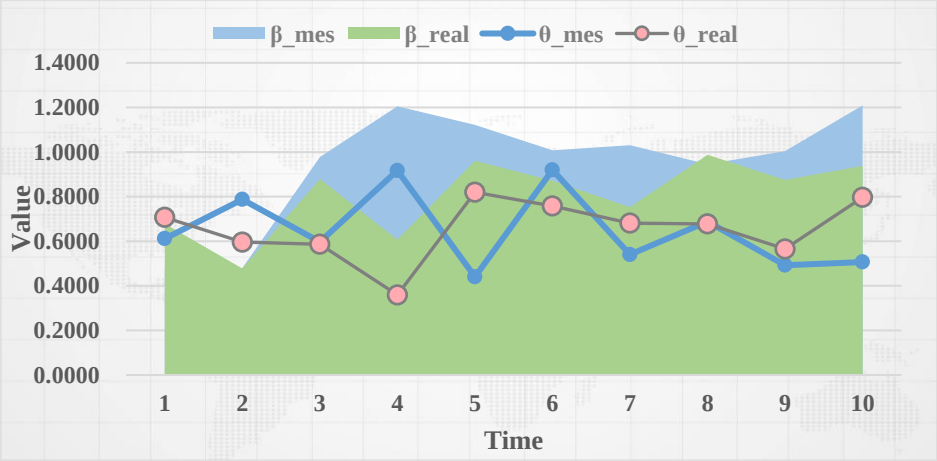

Figure 9: Attitude estimation of quadrotor UAV

5. Conclusions

This paper mainly studies the attitude control of rotorcraft. On the basis of hardware platform, we study the algorithm of quadrotor aircraft, including attitude angle algorithm and PID control algorithm. Finally, we write embedded software to write communication protocol and algorithm into STM32, and complete the design of the whole system. The attitude information of the aircraft is obtained by experiment and applied to the practical control in the future. The controller parameters obtained from simulation are applied to the actual control, and the control is carried out on the flight research platform, and the ideal flight effect is obtained.

In this paper, the force analysis of the four-rotor aircraft is carried out, and the dynamic model of the aircraft is obtained through the analysis of external force and external moment balance. The control effect of each channel interferes little with each other, independent control can be realized, and the speed and stability of control basically reach the design goal. The angular motion is analyzed by the law of rigid body rotation, and the angular motion equation is established. According to the linear motion and angular motion equations, the dynamic equations are obtained. This paper appropriately derives and merges the angular motion equation to form a more intuitive angular motion equation.

This paper proves through experiments that the real-time performance of the algorithm is improved after the saliency detection method is introduced in the target recognition stage, and a simple error analysis is made on the results of the ranging. By recording and analyzing the running track and characteristics of the tag mark, predict the next tag mark. In the case of ensuring the recognition rate, the resolution is maximized to improve the accuracy of recognition, and the position information obtained by prediction is used to interpolate the positioning information to improve the frame rate of the positioning information. Aiming at the positioning of the rotor drone on the moving target in the air, using the parallax principle in binocular stereo vision, the distance information obtained is converted into position information through coordinates, the position of the target is judged, and the positioning effect is analyzed, which can meet the requirements of the air rotor requirements for drone positioning.

Acknowledgements

The project was supported by the Computer Subject Team Building Project, Huanggang Normal University.

References

[1] Sun T H , Tien F C , Tien F C , et al. Automated thermal fuse inspection using machine vision and artificial neural networks[J]. Journal of Intelligent Manufacturing, 2016, 27(3):639-651.
[2] Jiang H , Duerstock B S , Wachs J P . A Machine Vision-Based Gestural Interface for People With Upper Extremity Physical Impairments [J]. IEEE Transactions on Systems, Man, and Cybernetics: Systems, 2017, 44(5):630-641.

ISSN 2706-655X Vol.3, Issue 8: 25-38, DOI: 10.25236/IJFET.2021.030805

[3] Favret C , Sieracki J M . Machine vision automated species identification scaled towards production levels [J]. Systematic Entomology, 2016, 41(1):133-143.
[4] Li P , Zheng M , Jing J . Measurement system of garment dimension based on Machine Vision [J]. Wool Textile Journal, 2017, 45(3):42-47.
[5] Fernandez-Robles L , Azzopardi G , Alegre E , et al. Machine-vision-based identification of broken inserts in edge profile milling heads[J]. Robotics and Computer-Integrated Manufacturing, 2017, 44(4):276-283.
[6] Carroll J . Machine vision lighting companies address niche imaging requirements [J]. Vision Systems Design, 2019, 24(6):22-27.
[7] Hosseinpour S , Ilkhchi A H , Aghbashlo M . An intelligent machine vision-based smartphone app for beef quality evaluation [J]. Journal of food engineering, 2019, 248(5):9-22.
[8] Saravanan D . Machine vision technique for detection of cotton contaminations [J]. Man-Made Textiles in India, 2019, 47(12):409-413.
[9] Cubero S , Lee W S , Aleixos N , et al. Automated Systems Based on Machine Vision for Inspecting Citrus Fruits from the Field to Postharvest—a Review[J]. Food & Bioprocess Technology, 2016, 9(10):1623-1639.
[10] Xiangyang Z , Jinwu Z , Zhihong Q , et al. Straight Line Detection Algorithm in Cigarette Packet Stamp Inspection Based on Machine Vision Technology[J]. Tobacco ence & Technology, 2008, 49(7):105-109.
[11] Dawood T , Zhu Z , Zayed T . Machine vision-based model for spalling detection and quantification in subway networks [J]. Automation in Construction, 2017, 81(9):149-160.
[12] Amraei S , Abdanan Mehdizadeh S , Salari S . Broiler weight estimation based on machine vision and artificial neural network [J]. British Poultry Science, 2017, 58(2):200-205.
[13] Tang W , Tian L , Zhao X . Research on displacement measurement of disk vibration based on machine vision technique [J]. Optik - International Journal for Light and Electron Optics, 2016, 127(8):4173-4177.
[14] Naderiparizi S , Kapetanovic Z , Smith J R . Battery-Free Connected Machine Vision with WISPCam [J]. Mobile computing and communications review, 2016, 20(1):10-13.
[15] Shi L , Ren H , Wang J , et al. Latin square design for chip length machine vision measurement system analysis[J]. Quality Engineering, 2016, 28(4):381-387.
[16] You F , Li Y H , Huang L , et al. Monitoring drivers' sleepy status at night based on machine vision[J]. Multimedia Tools & Applications, 2017, 76(13):14869-14886.
[17] Xi Q , Rauschenbach T , Daoliang L . Review of Underwater Machine Vision Technology and Its Applications [J]. Marine Technology Society Journal, 2017, 51(1):75-97.
[18] Yang A , Gao X , Li M . Design of apochromatic lens with large field and high definition for machine vision [J]. Appl Opt, 2016, 55(22):5977-5985.
[19] Li-Ying C , San-Peng H E , Qian L , et al. Quantifying muskmelon fruit attributes with A-TEP-based model and machine vision measurement[J]. Journal of Integrative Agriculture, 2018, 17(006):1369-1379.
[20] Chu H H , Wang Z Y . A study on welding quality inspection system for shell-tube heat exchanger based on machine vision [J]. International Journal of Precision Engineering & Manufacturing, 2017, 18(6):825-834.
[21] Sun G , Li Y , Zhang Y , et al. Nondestructive measurement method for greenhouse cucumber parameters based on machine vision[J]. Engineering in Agriculture Environment & Food, 2016, 9(1):70-78.
[22] Hashemzadeh M , Farajzadeh N . A Machine Vision System for Detecting Fertile Eggs in the Incubation Industry [J]. International Journal of Computational Intelligence Systems, 2016, 9(5):850-862.
[23] Jie S , Yinya L , Guoqing Q , et al. Machine vision based passive tracking algorithm with intermittent observations[J]. Journal of Huazhong University of ence and Technology (Natural ence Edition), 2017, 45(6):33-37.
[24] Tsai D M , Hsieh Y C . Machine Vision-Based Positioning and Inspection Using Expectation–Maximization Technique [J]. IEEE Transactions on Instrumentation & Measurement, 2017, 66(11):2858-2868.
[25] Kamaev A N , Sukhenko V A , Karmanov D A . Constructing and visualizing three-dimensional sea bottom models to test AUV machine vision systems [J]. Programming and Computer Software, 2017, 43(3):184-195.
[26] Liu D , Lu Z , Cao T , et al. A real-time posture monitoring method for rail vehicle bodies based on machine vision [J]. Vehicle System Dynamics, 2017, 55(6):853-874.
[27] Moore A J , Schubert M , Dolph C , et al. Machine Vision Identification of Airport Runways with

ISSN 2706-655X Vol.3, Issue 8: 25-38, DOI: 10.25236/IJFET.2021.030805

Visible and Infrared Videos[J]. Journal of Aerospace Computing, Information and Communication, 2016, 13(7):1-12.
[28] Nattharith P , Guzel M S . Machine vision and fuzzy logic-based navigation control of a goal-oriented mobile robot [J]. Adaptive Behavior, 2016, 24(3):168-180.
[29] Chen J , Gu Y , Lian Y , et al. Online recognition method of impurities and broken paddy grains based on machine vision[J]. Nongye Gongcheng Xuebao/Transactions of the Chinese Society of Agricultural Engineering, 2018, 34(13):187-194.